GEBZE TECHNICAL UNIVERSITY

**Acta Materialia Turcica**

Volume 4, June 2020, Pages 39-47

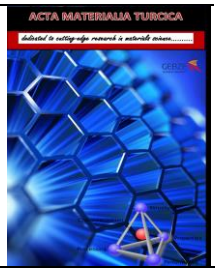


# Modelling of Deteriorated Electrical Steel Properties Due to Laser Cutting Procedure

M.A. ILGAZ*, S. COROVİC, D. MAKUC, A. ALİC, M. VUKOTİC, D. MİLJAVEC

*University of Ljubljana, Faculty of Electrical Engineering, Trzaska 25, 1000 Ljubljana, Slovenia*

**Abstract:**

The quality and efficiency of electrical machines are key factors towards improvement of the drive performance. Manufacturing processes have a significant impact on the efficiency of electrical machines. There are different manufacturing techniques such as mechanical cutting, laser cutting, electrical discharge machining etc. Each cutting techniques may cause a deformation near edges of the cutting area that may severely affect the properties of the B-H curve of the ferromagnetic materials. Thus it is important to predict approximately the extension of the damaged area. In this study we have developed an approach based on finite element method using COMSOL Multiphysics simulation software to evaluate the deformation caused by laser cutting on the edges of the ferromagnetic material.

**Keywords:** Laser Cutting; Ferromagnetic Materials; Deformation; B-H Curve

**DOI:**

## 1. INTRODUCTION

In order to manufacture electrical machines of high quality, the appropriate manufacturing processes of the ferromagnetic material and other components should be carefully implemented. One of the critical step of the machine manufacturing is the cutting of the electrical steel. Usually one of the cutting techniques is performed such as mechanical cutting (such as punching, or shearing) [1-5], laser cutting [2, 5-7] (different type of laser such as $CO_2$ laser, FKL laser etc.), electrical discharge machining (EDM) [4], water-jet cutting [8], wire electrical erosion [9], and photo-corrosion [10]. Laser cutting and mechanical cutting are the most frequently used in the industry because of their advantages. In general, the laser cutting techniques is suitable for prototype design, but it is not convenient manufacturing process for mass production, while the mechanical cutting is widely preferred for mass production [11]. In [9] a comprehensive research was done to see the effects of the punching, laser, abrasive water jet and wire erosion techniques. The results show that the mechanical cutting causes a plastic deformation and rounding, the laser cutting causes burr and dross formation while abrasive water jet provokes the burr formation on the cut edge [9]. In addition, oxidation was noticed on the shear edge by wire erosion technique [9]. On the other hand, in [10] the author claims that the photo-corrosion is the least damaging technique on the ferromagnetic material. A large number of authors agree that the cutting process technique has a significant influence on the magnetic properties of the ferromagnetic material [10-15]. Especially, the B-H curve of the material deteriorates after the cutting process. The cutting is not only step affecting the B-H curve properties of the ferromagnetic material, some other mechanical steps such as welding [16] or interlocking [17] also have an impact and may change the B-H curve of the ferromagnetic material.

As it is already described above the cutting process causes deformation on the edges of the ferromagnetic material. The deformation on the ferromagnetic material depends on the several parameters which are closely related to the cutting process. In this article, we present our analytical and numerical modeling approach for



*Corresponding Author E-mail: mehmet.ilgaz@fe.uni-lj.si

Acta Materialia Turcica

Volume 4, June 2020, Pages 39-47

simulating the measurement procedure of the ferromagnetic properties of the ring-core (i.e. toroid core) sample. We modeled the ferromagnetic material as a ring-core sample made of ferromagnetic material SURA M400-50A [18]. Based on this we present an algorithm for modelling of the ring-core sample specifications and show how the degradation of the material affects its B-H curve due to the cutting process.

## 2. METHODS

In the present article we used a ring-core with the size of 160-146-6 mm. The idea is to analytically and numerically simulate the measurement procedure of the ferromagnetic properties. In order to achieve this, we built a model of a ring-core shaped ferromagnetic sample with material properties (M400-50A) from the previous work [19]. We designed the model as a ring-core with the deformations near cutting edges and we have inserted primary and secondary windings around the core. The ring-core is composed of primary and secondary windings and there are thin layers of deformations on the edges of the ferromagnetic core caused by the cutting. The illustration of the typical configuration of the ring-core after the manufacturing process is shown in Figure 1.

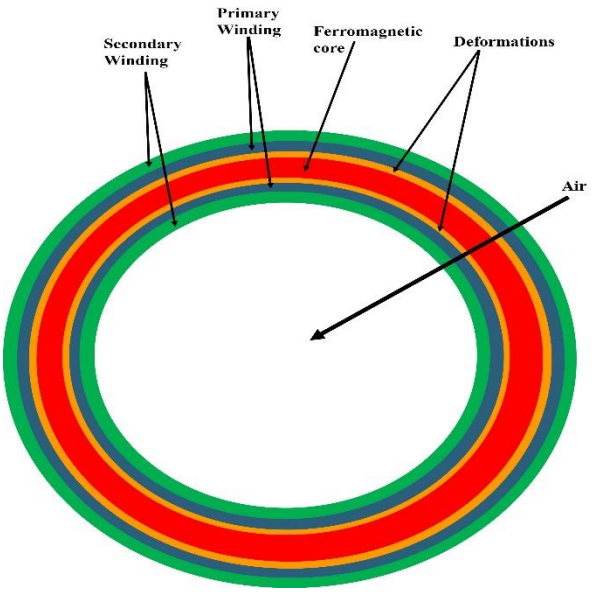


**Figure 1.** Illustration of the typical configuration of a ring-core after cutting process.

We developed/built up a model in the COMSOL Multiphysics software [20]. Namely, COMSOL Multiphysics is a powerful tool for design and simulation of electromagnetic devices based on defined geometries, experimental parameters such as material properties, input parameters (such as frequency, voltage etc.) [20]. The COMSOL Multiphysics runs the simulation using finite element method (FEM). The deformation has an impact on the overall B-H curve of the core. In other words, the healthy area has the same B-H curve as after cutting but the deformed area has a poor B-H curve and these poor ferromagnetic behaviors have an influence on overall B-H curve of the ring-core. We assume that the impact mainly depends on the size of the ring-core. This means that the deformation has serious consequences when the ring-core has a smaller size. Therefore, in our approach the dimensions of the ring-core with the same deformation is varied to see the impact of the deformation on the B-H curve.

One of the main challenges of the simulation work is that we should develop an approach to find the value of the B-H curve of the deformed area. For the healthy material, the B-H curve is given/measured by the datasheet but on the other hand for the deformed area, the B-H curve is changed due to mechanical and thermal stress and other factors of the cutting. We developed our method to make an assumption to define the B-H curve of the damaged material. Our approach is based on a pre-assumption of the B-H curve. We approximately describe the B-H curve with a mathematical equation and then optimize the coefficients of the equation for interpolation. In this part, we describe our algorithm/approach to determine the B-H curve of the deformed area on the ferromagnetic material.

The B-H curve approximation of the algorithm is designed to be compatible with COMSOL Multiphysics. The simulation software requires definition of the input parameters such as the number of turns of the windings ($N_1$ and $N_2$) materials defined for the ring-core and coils, the operating frequency, input voltage etc. Another necessary input values are the dimensions of the ring-core, deformed area (if applicable) etc. After defining all required parameters and generation of finite element mesh, the COMSOL Multiphysics runs the simulation and provide the results such as induced voltage, magnetizing current, output B-H curve of the ring-core, magnetic field distribution in the model. MATLAB software is used to process the data obtained from COMSOL Multiphysics (i.e. LiveLink™ for MATLAB was used).



*Corresponding Author E-mail: mehmet.ilgaz@fe.uni-lj.si

Acta Materialia Turcica

Volume 4, June 2020, Pages 39-47

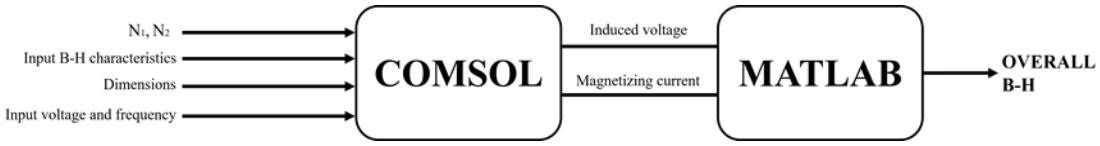


**Figure 2.** The input and output parameters analyzed with the COMSOL Multiphysics and MATLAB.

The working principle of the COMSOL Multiphysics and MATLAB is depicted in Figure 2.

There are various mathematical approximations to determine the B-H curve but due to the simplicity, the exponential approximation is selected [21]. The exponential approximation is done according to the equation 2.1.

$$B = a * \exp(b * H) + c * \exp(d * H) \qquad (2.1)$$

where the a, b, c, and d are the coefficients of the B-H curve to be determined with the algorithm, H is the magnetic field (A/m) and B is magnetic flux density (T). According to curve fitting toolbox of the MATLAB, the parameters are obtained as indicated below:
a=1.418; b= 2.349e-05; c= -2.137; d= -0.01466.

The approximation data and the manufacturer datasheet values [18] of M400-50A are illustrated in Figure 3.

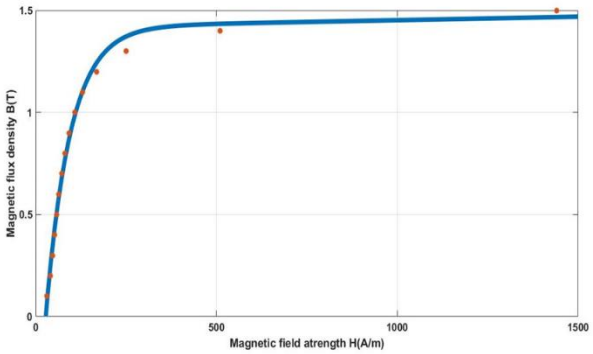


**Figure 3.** B-H curve approximation by using exponential approach for M400-50A.

According to results shown in Figure 3, we can also approximate the B-H curve of the deformed area of the ring-core and express it with a mathematical expression.

This helps us to determine our approach to find the B-H curve of the deformed area of the ring-core. The overall B-H curve of the ring-core depends on the relative dimensions of the deformation. The overall B-H of the ring-core is calculated by the magnetizing current and the induced voltage in the secondary coil. The magnetic field H is calculated as in equation 2.2,

$$H = N * \frac{I}{l_{ef}} \qquad (2.2)$$

here N is the number of turns, $l_{ef}$ is the effective magnetic path and I is the magnitude of the magnetizing current. The magnetic flux density B is calculated as in equation 2.3,

$$B(t) = -\frac{1}{NA}\int V(t)dt, \qquad (2.3)$$

where V is the induced voltage and A is the area of the ring-core. The algorithm for determination of the B-H curve of the degraded area is composed of the several steps. The first step is to measure the B-H curve of a very large ring-core because the deformed area has a negligible effect on the large ring-core. The next step is to measure the B-H curve of the overall ring core having smaller dimensions where the degraded area has a larger impact on the overall B-H curve of the ring-core. After obtaining the data next steps are based on the algorithm design. The initial B-H curve (dummy B-H curve) of the degraded area of the ring-core with smaller size is defined and together with the healthy B-H curve are inserted in the FEM model to obtain the simulation result. Both results are then compared. The algorithm is designed in such a way to alternate the parameters in order to suit each other. The flowchart of the algorithm is shown in Figure 4.



Corresponding Author E-mail: mehmet.ilgaz@fe.uni-lj.si

Acta Materialia Turcica

Volume 4, June 2020, Pages 39-47

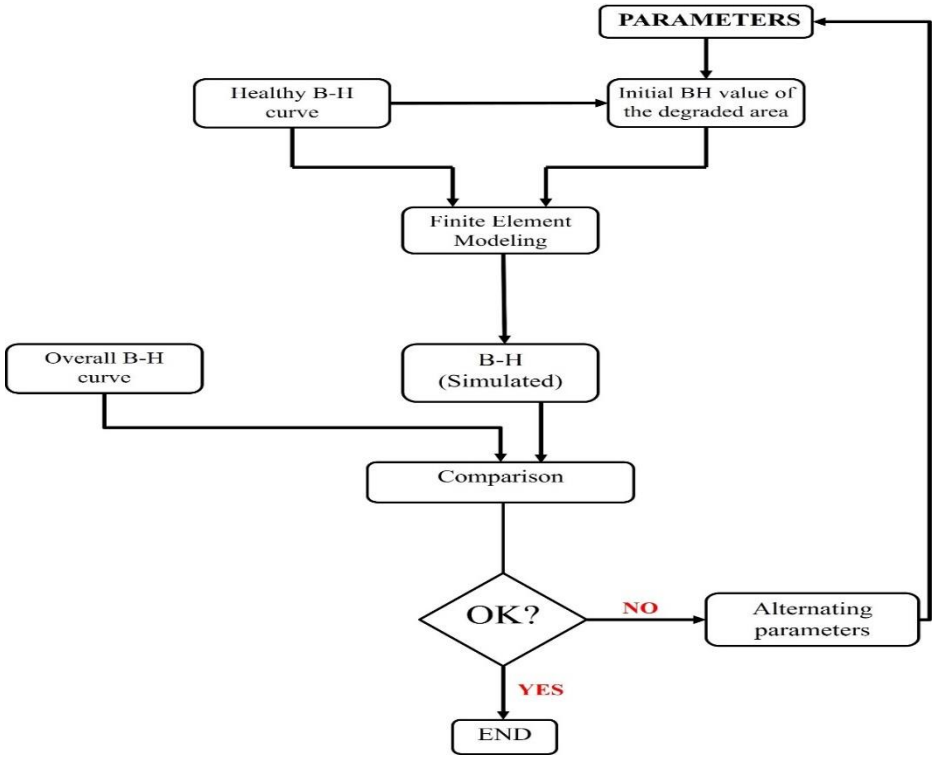


**Figure 4.** The flowchart describes the steps of the proposed algorithm to find the B-H curve of the degraded area.

The B-H curve of the ferromagnetic material are specified by two parameters: $X_B$ and $X_H$ as stated in equations 2.4, and 2.5.

$$B = X_B * B_i, \quad (2.4)$$

$$H = X_H * H_i, \quad (2.5)$$

where $X_B$ and $X_H$ are coefficients for varying the magnetic flux density B and magnetic field strength H of the deformed area, $B_i$ and $H_i$ are the values of the healthy material. For the healthy ferromagnetic material the values of the coefficients are $X_B = 1$ and $X_H = 1$.

## 3. RESULTS

### 3.1 Modeling of uniform/undeformed and deformed ferromagnetic sample

The modelling of magnetic behavior of ferromagnetic material is significant step towards evaluation and prediction of the electrical machine quality. These modelling and analysis are required to develop high-performance electrical machines with a low cost [22]. In the Table 1, the results of the iron magnetic quantities calculation of the ring-core are presented when the deformation area has a coefficient of $X_H = 1.33$.

**Table 1:** Iron magnetic quantities for non-deformed and deformed ring-core with the $X_H = 1.33$.

| $B_1$ / [T] | $H_1$ / [A/m] | $H_2$ / [A/m] | $\mu_{r1}$ | $\mu_{r2}$ | $U_{p1} = U_{p2}$ /[V] |
|---|---|---|---|---|---|
| 0,1 | 34 | 45,22 | 2489 | 1760 | 0,012 |
| 0,2 | 43 | 57,19 | 3515 | 2784 | 0,022 |
| 0,3 | 53 | 70,49 | 4496 | 3388 | 0,033 |
| 0,4 | 62 | 82,46 | 5389 | 3862 | 0,045 |
| 0,5 | 70 | 93,1 | 6151 | 4276 | 0,055 |
| 0,6 | 78 | 103,74 | 6749 | 4605 | 0,066 |
| 0,7 | 86 | 114,38 | 7206 | 4872 | 0,078 |
| 0,8 | 95 | 126,35 | 7554 | 5041 | 0,0885 |
| 0,9 | 105 | 139,65 | 7793 | 5131 | 0,0989 |
| 1 | 119 | 158,27 | 7782 | 5035 | 0,1095 |



*Corresponding Author E-mail: mehmet.ilgaz@fe.uni-lj.si

Acta Materialia Turcica

Volume 4, June 2020, Pages 39-47

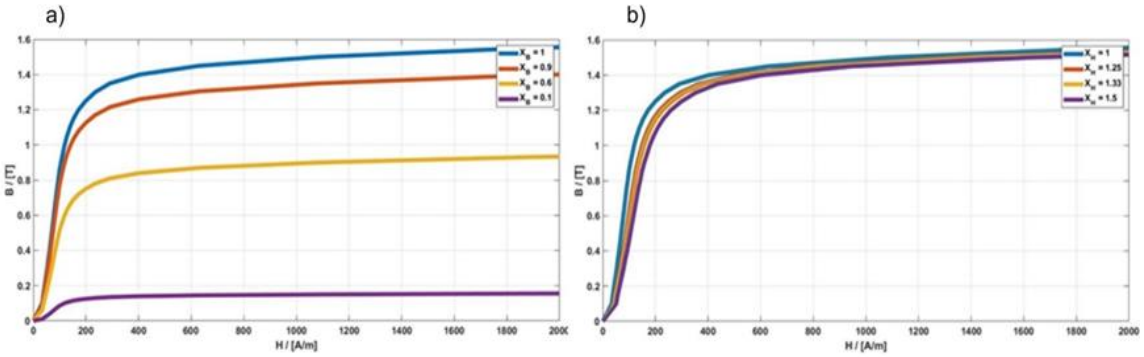


**Figure 5. a)** B-H curve with different coefficients of B when the H is fixed to healthy values **b)** B-H curve with different coefficients of H when the B is fixed to healthy values.

In the Table 1, the calculations are given for the material of M400-50A. B1 is the magnetic flux density, $H_1$ and $H_2$ are the magnetic field strength and where $H_1$ shows the fully healthy material and $H_2$ shows the fully degraded material. $U_{p1}=U_{p2}$ are the input voltages, and $\mu_{r1}$ and $\mu_{r2}$ are the magnetic relative permeability's of the healthy and degraded materials, respectively.

### 3.2 Modeling of ferromagnetic sample with introduced deformation area by technological/manufacturing process

In order, better understand the influence of the presence of the deformation on the ferromagnetic properties of the sample we studied the behavior of the B-H curve of the
degraded area, by varying the values of the coefficients $X_B$ and $X_H$. The results are given in the Figure 5.

The B-H curve shown in Figure 5 are obtained when the X_B coefficient is altered by different values such as 1 (no deformation), 0.9, 0.6 and 0.1 and X_H coefficient is altered by 1 (no deformation), 1.33, 1.25 and 1.5. This means that when the X_B is reduced with the constant $X_H$ and $X_H$ is increased when the $X_B$ is fixed, the material needs more magnetic field strength H (A/m) to obtain a higher magnetic flux density B (T). In other words, the deformed area has deteriorated properties on the B-H curve and those damaged properties affect the overall B-H curve of the ring-core.

In order to simulate/model the magnetic properties of the ferromagnetic material processed with laser cutting technological process used in electrical machines we built FEM models of ring-core samples with the introduced/added deformed area (where the deformation width is 1 mm on the edges of the ring-core sample). In the Figure 6, the deformed area with different $X_B$ and $X_H$ values are given.

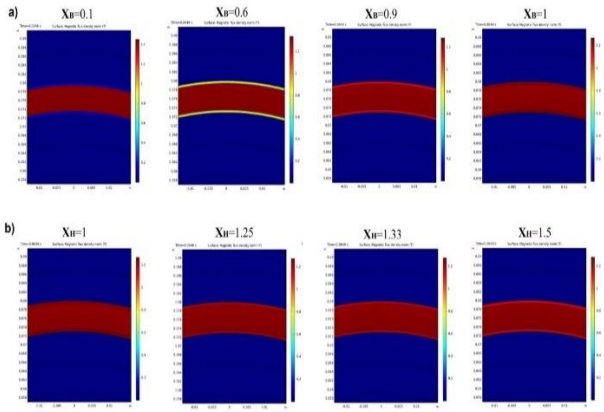


**Figure 6.** Magnetic flux density with changed coefficients: **a)** $X_B$ = 0.1, $X_B$ = 0.6, $X_B$ = 0.9, $X_B$ = 1(no deformation) and **b)** $X_H$ =1 (no deformation), $X_H$ =1.25, $X_H$ =1.33, $X_H$ =1.5 when maximum value of the magnetic flux density is obtained.

As described previously in the flowchart shown in Figure 4, first of all we should define the input parameters in COMSOL Multiphysics to run the simulation. We have used a 160-146-6 mm ring-core with primary and secondary windings having 150 number of turns. The input voltage was 2.5 V with 50 Hz frequency. The ring-core has a SURA M400-50A material properties and the windings are defined as copper in COMSOL Multiphysics. The B-H curve of the healthy M400-50A is defined in the simulation software. We have used the data



Corresponding Author E-mail: mehmet.ilgaz@fe.uni-lj.si

Acta Materialia Turcica

Volume 4, June 2020, Pages 39-47

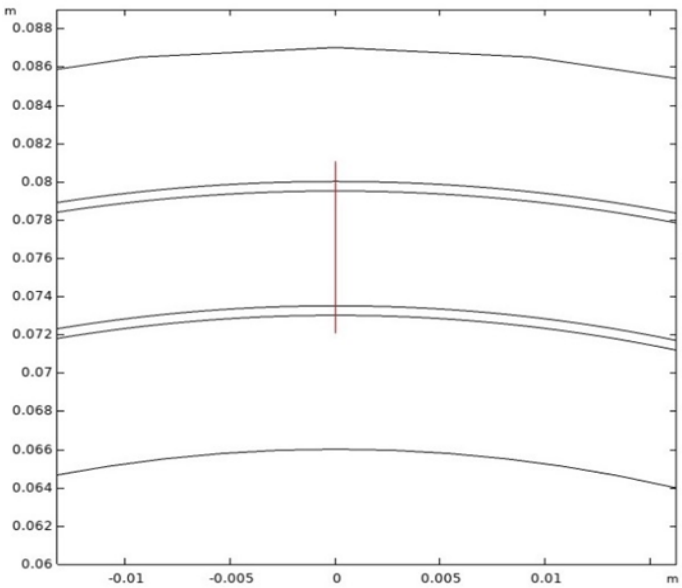


**Figure 7.** The cut line on the ring-core along which the results of B are shown.

from the datasheet of M400-50A [18] to define the B-H curve of the ring-core. For degraded area, we should alter the $X_B$ values while we fix the $X_H$ to define the 'dummy' B-H curve. We show how the magnetic flux density is changing as the damaged properties of the deformed area is increased by coefficient of the $X_B$. We selected the moment when the B value is at maximum. In Figure 7 we defined the cut line along which we displayed the results of B in Figure 8.

In the Figure 8, we demonstrate how the B is changing with the dominance of the deformed area (in other words we analyzed the region where the $X_B$ is decreased with fixed $X_H$ and when $X_H$ is increased with fixed $X_B$).

Figure 8.a shows the comparison of magnetic flux density distributions (B) in the ferromagnetic samples with different B-H curves in the deformed area. So the lowest value of B occurred in the sample with the B-H curve of the deformed area with the lowest multiplying factor $X_B = 0.1$. On the other hand, the Figure 8.b shows that the B has the lowest value with the highest $X_H$ factor ($X_H = 1.5$). Further, in the Figure 9, we show how the magnetizing current changes with the different dominance of the deformation of the $X_B$ and $X_H$ factors.

Based on our results, we show that the influence of $X_B$ is more pronounced compared to the influence of factor $X_H$ (the magnetizing current in Figure 9.b is almost is equal for different values of $X_H$ factor) .

The Figure 9.a shows that the magnetizing current is increased when the deformation is more dominant. In the Figure 10, we provide the B-H curve of the overall ring-core without deformation and with deformation with different values of $X_B$ and $X_H$ .

The Figure 10.a shows that the slope of the output B-H curve changes when the $X_B$ is decreased. On the other hand, the results in Figure 10.b show that due to the increase of factor $X_H$ up to 50%, the output B-H curve remained almost unchanged.



*Corresponding Author E-mail: mehmet.ilgaz@fe.uni-lj.si

Acta Materialia Turcica

Volume 4, June 2020, Pages 39-47

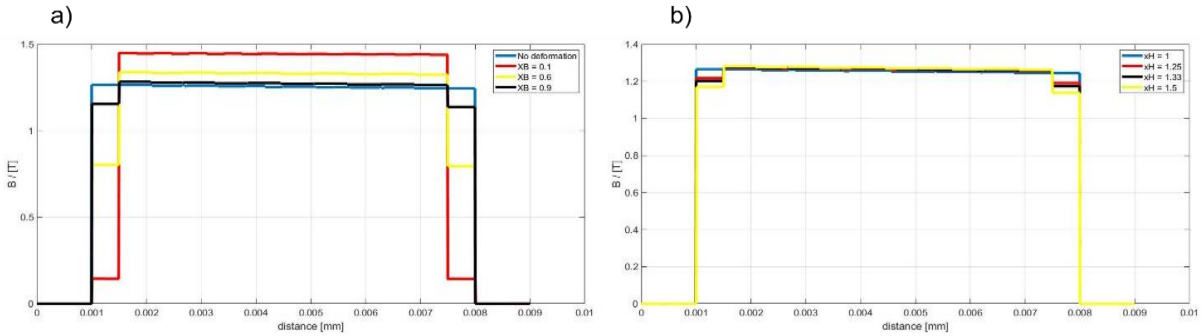


**Figure 8.** Magnetic flux density along the cut line over the ring-core for the variations of: **a)** $X_B$ and **b)** $X_H$.

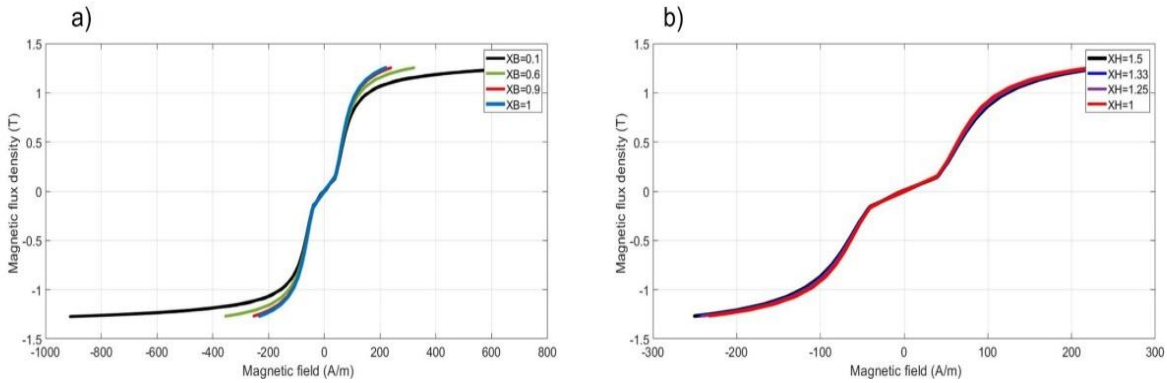


**Figure 9.** Magnetizing current of the primary coil over time obtained from the no deformation ring-core and the ring-core with deformation having different coefficients for variations of: **a)** $X_B$ and **b)** $X_H$.

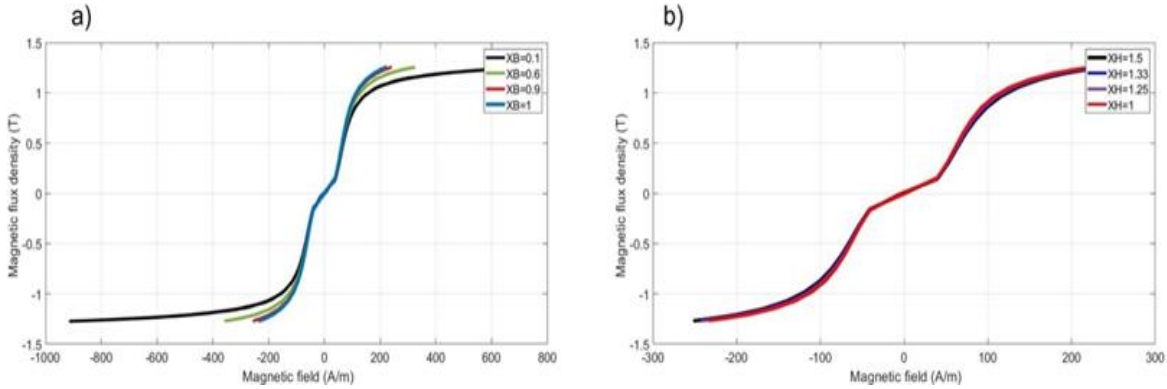


**Figure 10.** Overall B-H curve of the ring-core with different values of: **a)** $X_B$ and **b)** $X_H$.



*Corresponding Author E-mail: mehmet.ilgaz@fe.uni-lj.si

Acta Materialia Turcica

Volume 4, June 2020, Pages 39-47

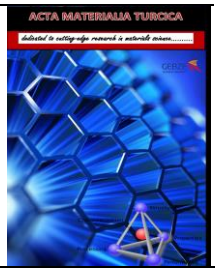

## 4. DISCUSSION

According to the obtained simulation results, we have shown that our algorithm approach can be successfully used for identification of the B-H curve of the degraded area near the edges of the ferromagnetic material due to the cutting. The deformation area has a negligible effect on the ring-core sample with larger dimensions but on the other hand the overall B-H curve of the ring-core sample with smaller dimensions can be significantly affected. This deformation is based on a large number of parameters but in this work, our simulations do not rely on any cutting technique since the main objective was to simplify the algorithm. In this study, we only take into consideration the deformation size and the dominance (by varying the $X_B$ and $X_H$ parameters) of the deformation on the ring-core to see its effect on the B, B-H curve and the magnetizing current. There are also other factors that may have an impact on the overall B-H curve such as: the type of the cutting technique, welding, interlocking etc. In order to further simplify the calculations, we approached only one ring-core size for the same deformation size used in the simulations to eliminate the unknowns as much as possible.

## 5. CONCLUSION

In this paper we have introduced our proposed algorithm based on the FEM to determine the B-H curve of the degraded material on the edges of the ring-core due to the cutting. The results obtained in this paper are the preliminary results of the finite element based modelling approach. In the future work, we intend to extend our algorithm with the experimental work. The future work will also include other factors such as interlocking and welding of the ring-core. The manufactured ring-core samples will be prepared in different dimensions with and without interlocking/welding and the experimental study will be done in a way to incorporate all phenomena and further on they will be compared with the measurements.

## 6. ACKNOWLEDGMENT

The authors acknowledge the project ID L2-8187 was financially supported by the Slovenian Research Agency. This work is part of the MOTZART, that is financed by the Republic of Slovenia and the European Union under the European Regional Development Fund.

## 7. REFERENCES

[1] H. Naumoski, A. Maucher, L. Vandenbossche, S. Jacobs, U. Herr, and X. Chassang, Magneto-optical and field-metric evaluation of the punching effect on magnetic properties of electrical steels with varying alloying content and grain size, 4th International EDPC, 1-9 (2014). **DOI:** 10.1109/EDPC.2014.6984398.

[2] M. Bali, and A. Muetze, Influences of $CO_2$ Laser, FKL Laser, and Mechanical Cutting on the Magnetic Properties of Electrical Steel Sheets, IEEE Trans. Ind. Appl. 51 (6), 4446-4454 (2015).
**DOI:** 10.1109/TIA.2015.2453136.

[3] H. Naumoski, A. Maucher, and U. Herr, Investigation of the influence of global stresses and strains on the magnetic properties of electrical steels with varying alloying content and grain size, 5th International EDPC, 1-8 (2015). **DOI:** 10.1109/EDPC.2015.7323206.

[4] V. Manescu (Paltanea), G. Paltanea, H. Gavrila, and G. Scutaru, The effect of mechanical and electrical discharge cutting technologies on the magnetic properties of non-oriented silicon iron steels. Electrotech. Et energ. 60 (1), 59-68 (2015).

[5] E. G. Araujo, J. Schneider, K. Verbeken, G. Pasquarella, and Y. Houbaert, Dimensional effects on magnetic properties of fe-si steels due to laser and mechanical cutting, IEEE Trans. Magn. 46 (2), 213-216 (2010).
**DOI:** 10.1109/TMAG.2009.2034124.

[6] H. Naumoski, B. Riedmüller, A. Minkow, and U. Herr, Investigation of the influence of different cutting procedures on the global and local magnetic properties of non-oriented electrical steel, J. Magn. Magn. Mater. 392, 126-133 (2015).
**DOI:** 10.1016/j.jmmm.2015.05.031.

[7] A. Belhadj, P. Baudouin, F. Breaban, A. Deffontaine, M. Dewulf, and Y. Houbaert, Effect of laser cutting on microstructure and on magnetic properties of grain non-oriented electrical steels, J. Magn. Magn. Mater. 256 (1-3), 20–31 (2003).
**DOI:** 10.1016/S0304-8853(01)00937-4.



*Corresponding Author E-mail: mehmet.ilgaz@fe.uni-lj.si

GEBZE TECHNICAL UNIVERSITY

**Acta Materialia Turcica**

Volume 4, June 2020, Pages 39-47

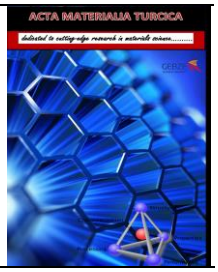

[8] A. Schoppa, H. Louis, F. Pude and Ch.von Rad, Influence of abrasive waterjet cutting on the magnetic properties of non-oriented electrical steels, J. Magn. Magn. Mater. 254-255, 370-372 (2003).
**DOI:** 10.1016/S0304-8853(02)00882-X.

[9] S. Bayraktar, and Y. Turgut, Effects of different cutting methods for electrical steel sheets on performance of induction motors, J. Eng. Manuf. 232, 1287-1294 (2016).
**DOI:** 10.1177/0954405416666899.

[10] M. Emura, F.J.G. Landgraf, W. Ross, and J.R. Barreta, The influence of cutting technique on the magnetic properties of electrical steels, J. Magn.Magn. Mater. 254-255, 358–360 (2003).
**DOI:** 10.1016/S0304-8853(02)00856-9.

[11] M. Hofmann, H. Naumoski, U. Herr, and H. Herzog, Magnetic properties of electrical steel sheets in respect of cutting: Micromagnetic analysis and macromagnetic modeling, IEEE Trans. Magn. 52 (2), 1-14 (2016), Art no. 2000114.
**DOI:** 10.1109/TMAG.2015.2484280.

[12] T. P. Holopainen, P. Rasilo, and A. Arkkio, Identification of magnetic properties for cutting edge of electrical steel sheets, IEEE Trans. Ind Appl. 53 (2) 1049-1053 (2017).
**DOI:** 10.1109/TIA.2016.2638405.

[13] M. Bali, and A. Muetze, The degradation depth of non-grain oriented electrical steel sheets of electric machines due to mechanical and laser cutting: A state-of-the-art review, IEEE Trans. Ind. Appl. 55 (1), 366-375 (2019).
**DOI:** 10.1109/TIA.2018.2868033.

[14] G. Loisos, and A. J. Moses, Effect of mechanical Nd: YAG laser cutting on magnetic flux distribution near the cut edge of non-oriented steels, in J. Mater. Process. Technol. 161 (1-2), 151-155 (2005).
**DOI:** 10.1016/j.jmatprotec.2004.07.061.

[15] Y.Kurosaki, H. Mogi, H. Fujii, T. Kubota, and M. Shiozaki, Importance of punching and workability in non-oriented electrical steel sheets, J. Magn. Magn. Mater. 320 (20), 2474-2480 (2008).
**DOI:** 10.1016/j.jmmm.2008.04.073.

[16] A. Krings, S. Nategh, O. Wallmark, and J. Soulard, Influence of the welding process on the magnetic properties of a slot-less permanent magnet synchronous machine stator core. XXth International Conference on Electrical Machines, 1333-1338 (2012).
**DOI:** 10.1109/ICElMach.2012.6350050.

[17] S. Imamori, S. Steentjes, and K. Hameyer, Influence of interlocking on magnetic properties of electrical steel laminations, IEEE Trans. Magn. 53 (11), 1-4 (2017), Art no. 8108704.
**DOI:** 10.1109/TMAG.2017.2713446.

[18] Datasheet of SURA M400-50A. https://cogent-power.com/cms-data/downloads/m400-50a.pdf. [accessed 06 April 2020].

[19] M. Breznik, V. Gorican, A. Hamler, S. Corovic, and D. Miljavec, Analysis and identification of influential phenomena on iron losses in embedded permanent magnet synchronous machine, J. Electr. Eng. 68 (1), 23-30 (2017).
**DOI:**10.1515/jee-2017-0003.

[20] COMSOL Multiphysics 5.5. https://www.comsol.com/comsol-multiphysics. [accessed 06 April 2020].

[21] Q. Tang, Z. Wang, P. I. Anderson, P. Jarman and A. J. Moses, Approximation and prediction of AC magnetization curves for power transformer core analysis, IEEE Trans. Magn. 51 (5), 1-8 (2015).
**DOI:** 10.1109/TMAG.2014.2372672.

[22] H. Tanaka, K. Nakamura, and O. Ichinokura, Calculation of iron loss in soft ferromagnetic materials using magnetic circuit model taking magnetic hysteresis into consideration, J. Mag. Soc. Jpn., 39 (2), 65-70 (2015).
**DOI:** 10.3379/msjmag.1501R001.



*Corresponding Author E-mail: mehmet.ilgaz@fe.uni-lj.si